AD-A011 707

COAT MEASUREMENTS AND ANALYSIS

James E. Pearson

Hughes Research Laboratories

Prepared for:

Advanced Research Projects Agency
Rome Air Development Center

May 1975

195059

RADC-TR-75-101
Interim Report
May 1975

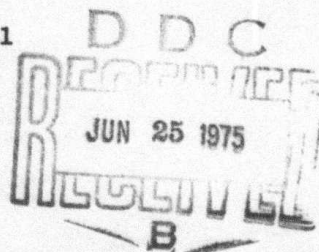COAT MEASUREMENTS AND ANALYSIS

Hughes Research Laboratories

Sponsored By
Defense Advanced Research Projects Agency
ARPA Order No. 1279

Approved for public release;
distribution unlimited.

The views and conclusions contained in this document are those
of the authors and should not be interpreted as necessarily
representing the official policies, either expressed or implied,
of the Defense Advanced Research Projects Agency or the U. S.
Government.

Rome Air Development Center
Air Force Systems Command
Griffiss Air Force Base, New York 13441

DDC

JUN 25 1975

RECEIVED

B

| REPORT DOCUMENTATION PAGE | | READ INSTRUCTIONS BEFORE COMPLETING FORM |
|---|---|---|
| 1. REPORT NUMBER RADC-TR-75-101 | 2. GOVT ACCESSION NO. | 3. RECIPIENT'S CATALOG NUMBER |
| 4. TITLE (and Subtitle) COAT MEASUREMENTS AND ANALYSIS | | 5. TYPE OF REPORT & PERIOD COVERED Quarterly Technical Report 2 1 Oct 74 - 31 Dec 74 |
| | | 6. PERFORMING ORG. REPORT NUMBER N/A |
| 7. AUTHOR(s) James E. Pearson | | 8. CONTRACT OR GRANT NUMBER(s) F30602-75-C-0001 |
| 9. PERFORMING ORGANIZATION NAME AND ADDRESS Hughes Research Laboratories 3011 Malibu Canyon Road Malibu CA 90265 | | 10. PROGRAM ELEMENT, PROJECT, TASK AREA & WORK UNIT NUMBERS 12790017 |
| 11. CONTROLLING OFFICE NAME AND ADDRESS Defense Advanced Research Projects Agency 1400 Wilson Blvd Arlington VA 22209 | | 12. REPORT DATE May 1975 |
| | | 13. NUMBER OF PAGES 45 |
| 14. MONITORING AGENCY NAME & ADDRESS(If different from Controlling Office) Rome Air Development Center (OCTM) Griffiss AFB NY 13441 | | 15. SECURITY CLASS. (of this report) UNCLASSIFIED |
| | | 15a. DECLASSIFICATION/DOWNGRADING SCHEDULE N/A |

16. DISTRIBUTION STATEMENT (of this Report)

Approved for public release; distribution unlimited.

17. DISTRIBUTION STATEMENT (of the abstract entered in Block 20, If different from Report)

Same

18. SUPPLEMENTARY NOTES
RADC Project Engineer:
Robert F. Ogrodnik (OCTM)
AC 315 330-4306

19. KEY WORDS (Continue on reverse side If necessary and Identify by block number)

COAT
Optical Radar
Laser Phased Arrays
Thermal Blooming Compensation

Active Optics
Adaptive Systems

20. ABSTRACT (Continue on reverse side If necessary and Identify by block number)
Compensation for thermal blooming distortions has been studied using multi-dither coherent optical adaptive techniques (COAT) in scaled laboratory experiments. An 18 element, visible wavelength, COAT system was able to effect only a small improvement in peak target irradiance for forced-convection blooming. Similar results were observed with a truncated Gaussian beam using a computer simulation which models atmospheric thermal blooming and uses a phase conjugate COAT control algorithm to adjust the transmitted beam phase. A factor of 2

DD FORM 1473 1 JAN 73    EDITION OF 1 NOV 65 IS OBSOLETE

correction was calculated, however, for an untruncated Gaussian transmitted beam. Refinements in the experimental apparatus to eliminate buoyancy effects are discussed and a design is presented for incorporating adaptive pointing and focus controls into the COAT system. Two designs for an artificial turbulence generator are presented along with a design for adding adaptive tracking and focus controls to the RADC/COAT system. Preliminary COAT studies without turbulence or blooming but with complex moving targets are reported. Normal COAT system operation is observed with all targets if the receiver has sufficient resolution and if the system signal-to-noise ratio is large enough for stable operation.

1a.

# COAT MEASUREMENTS AND ANALYSIS

Dr. James E. Pearson

2.

## PREFACE

This quarterly report was prepared by Hughes Research Laboratories, Malibu, California under Contract F30602-75-C-0001. It describes work performed from 1 October 1974 to 31 December 1974. The principal investigator and principal scientist is Dr. James E. Pearson. The project is part of the adaptive optics program at the Hughes Research Laboratories under the management of Dr. Joe A. Jenney.

# TABLE OF CONTENTS

**Preceding page blank**

5

# LIST OF ILLUSTRATIONS

**Preceding page blank**

# SUMMARY

The objectives of this research program are twofold: (1) study the ability of a multidither COAT system to compensate for thermal blooming and turbulence, particularly when it operates against complex multiple glint targets; (2) use a computer simulation to cross-check the experimental results and to derive design guidelines for high power COAT systems. This report summarizes the work performed during the second quarter of the contract from 1 October 1974 to 31 December 1974.

We have experimentally studied compensation for forced-convection thermal blooming using an 18-element COAT system which operates at $0.488 \mu m$. Operating against a single stationary glint target through an absorbing gas cell with a transverse wind, the COAT system has so far produced only small improvements in target irradiance. The experimental data, however, do not agree quantitatively with theory, partly because of buoyancy effects in the gas cell. We have modified the apparatus to minimize these effects for future experiments.

Computer simulations of COAT blooming compensation have been made using a phase conjugate correction algorithm. These simulations show a factor of 2 improvement in peak target irradiance when the transmitted beam has an untruncated Gaussian intensity profile. When the transmitted beam is a truncated Gaussian, however, the observed improvement is only 20%, in qualitative agreement with experiment.

Preliminary complex target studies have used moving multiple glint and moving diffuse targets. Normal operation of the COAT system is observed even when the receiver has only 1/3 the spatial resolution of the transmitter. The only exception is with a small receiver and a moving diffuse target, but this result is ambiguous because of a very low COAT system signal-to-noise ratio in the experiment.

Adaptive tracking and focus controls have been designed for the 18-element COAT system and are now under construction. These controls are also being incorporated into the computer simulation. Two designs for producing calibrated laboratory turbulence are being built. Both designs are simple phase screens; one screen design is fabricated by sputtering random

patches of $SiO_2$ onto quartz, and the other uses a photograph of a computer-generated phase screen.

Work during the next quarter will be in four areas: (1) completing modifications to the experimental apparatus, such as adaptive tracking and focus and turbulence generation; (2) additional thermal blooming studies aimed at better quantitative agreement with theory; (3) complex, moving glint target studies with blooming and turbulence; and (4) ongoing computer simulation work.

# I.   INTRODUCTION

## A.   Program Objectives

There are two primary objectives of this program. The first objective is to determine the performance limits of multidither coherent optical adaptive techniques (COAT) by performing scaled laboratory experiments which are designed to produce quantitative data on the nature of thermal blooming and turbulence and on the ability of multidither COAT to correct for these distortions, particularly when the target has many moving, time-varying glints. The second objective is to use computer simulation as a cross check on the experiments and as an analytical tool to derive design parameters for high power COAT systems.

## B.   Research Program Plan

The performance of multidither COAT has already been proved with an 18-element visible wavelength system developed and tested on DARPA/RADC Contract F30602-73-C-0248 which was concluded in July 1974. This same system is used for the laboratory experiments in this program. The computer simulation codes for atmospheric turbulence, thermal blooming, and the COAT system are being developed on DARPA/NOL Contract N60921-74-C-0249. The previous DARPA/RADC COAT contract also supplied a design for a gas absorption cell which will be used to simulate convection-dominated thermal blooming in the atmosphere.

The research program for this contract, illustrated in Fig. 1, runs from 2 July 1974 through 30 June 1975. The required oral presentation was made on 3 December 1974 as part of the DARPA/NOL Adaptive Optics Symposium held at Lincoln Laboratories.[1]  A contract amendment negotiated during the second contract quarter provides for the addition of auto-tracking and autofocus controls to both the RADC/COAT hardware and the Naval Ordnance Laboratories computer code. These additions should not interfere with other scheduled work, and so will take place from December 1974 through February 1975.
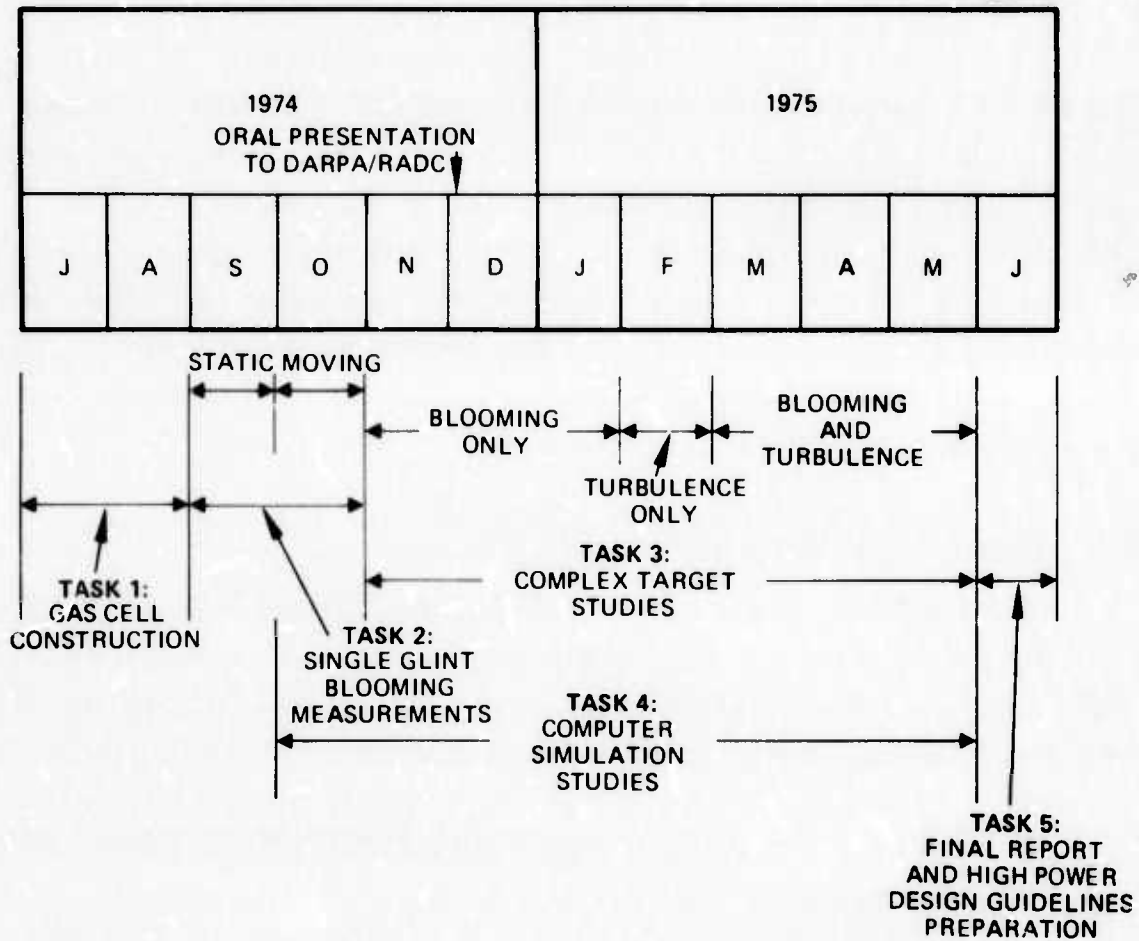
Fig. 1.  Research program plan showing COAT tasks and scheduling.

## II.   TECHNICAL ACCOMPLISHMENTS

### A.   Thermal Blooming — Experimental Studies

During this quarter we have concentrated on COAT measurements using a single fixed-glint target. All of the quantitative measurements were made using the forced-convection gas cell simulator discussed in the previous report.[2] We have also made some observations using a flowing liquid cell, but have not yet quantified these measurements.

#### 1.   Gas Cell

As indicated in the previous report,[2] the gas cell uses a small amount of $NO_2$ to absorb the 0.488 $\mu$m radiation transmitted by the COAT system and a second (buffer) gas at one atmosphere of pressure to produce the thermal blooming. This technique relies on efficient transfer of energy absorbed by the $NO_2$ to translational (heat) energy in the buffer gas in a time short compared to a convection time (for convection-dominated heat transfer). Based on estimated energy transfer rates and a calculated figure of merit,[3] we identified $SF_6$ and Xe as the best buffer gas candidates. Because of its significantly lower cost, $SF_6$ was tried first.

Much to our surprise and continuing puzzlement, the $SF_6$-filled gas cell produced an order of magnitude less blooming than expected. After convincing ourselves that there was no error in our calculations and that the $SF_6$ and $NO_2$ were thoroughly mixed, we abandoned the use of $SF_6$ and filled the cell with Xe (one fill requires about 4 liters of gas at one atmosphere). The Xe-$NO_2$ cell produced significant blooming with the available optical power but, as discussed below, still less than calculated.

All measurements were made using the arrangement shown in Fig. 2. The details of this setup have been previously discussed.[2] The first test was performed with no transverse wind to compare with earlier data taken with a thin static liquid cell.[2] The observed beam profiles are shown in Fig. 3. Note that at low power the far field patterns of the beams in each path are the same, indicating the identical optical quality of the two paths. The profiles shown in Fig. 3 are "A-scope" presentations. That is, the intensity distribution of the <u>entire beam</u> is shown in profile, not just a single trace through the center of the beam. Thus, all of the beam sidelobes can be seen.

13
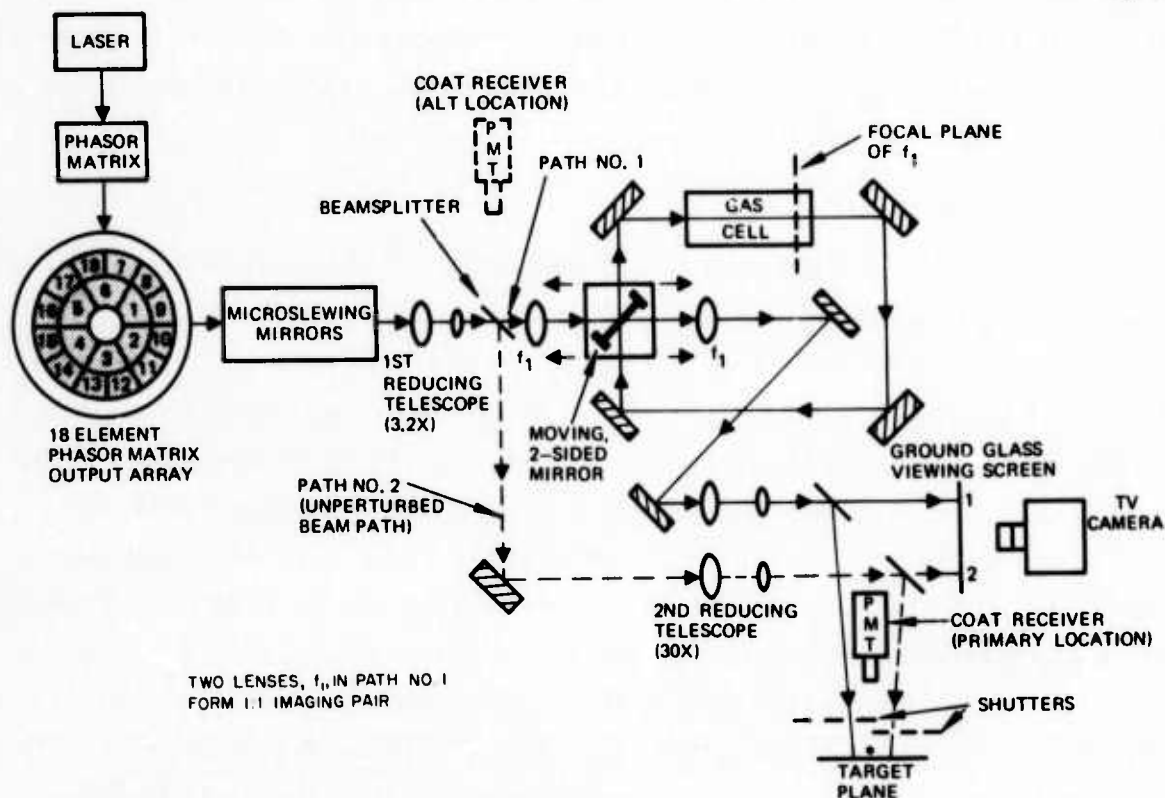
Fig. 2. Schematic of laboratory optics. Path No. 1 through the blooming cell and path No. 2 outside the cell are optically identical when the cell is not filled.

NO COAT CORRECTION

0 dB —
−3 dB —

(a)

0 dB —

(b)

0 dB —

(c)

COAT CORRECTION

0 dB —

(d)

0 dB —

(e)

0 dB —

(f)

LOW
POWER
NO
BLOOMING

MEDIUM
POWER
MODERATE
BLOOMING

HIGH
POWER
STRONG
BLOOMING

BLOOMED BEAM
(FAR−FIELD OF
CELL OUTPUT,
PATH NO. 1)

UNBLOOMED BEAM
(FAR−FIELD OF
CELL INPUT,
PATH NO. 2)

BLOOMED BEAM
(FAR−FIELD OF
CELL OUTPUT,
PATH NO. 1)

UNBLOOMED BEAM
(FAR−FIELD OF
CELL INPUT,
PATH NO. 2)

Fig. 3.   Far field beam profiles with no transverse wind in the gas
cell.   The left column of photographs, (a) through (c), is for
no COAT correction.   The right hand column, (d) through (f),
is with COAT correction.   Each picture shows two far field
beam profiles: the output of the gas cell (path No. 1 in Fig. 2)
and the input to the cell (path No. 2 in Fig. 2).

15

The observed blooming and COAT correction at higher powers is very similar to that observed with the static liquid cell (compare Fig. 3 to Fig. 9 of the previous report). Quantitatively, the observed COAT correction with the static gas cell is nearly identical to that with the liquid cell (see Fig. 11 of Ref. 2); that is, the COAT system increases the peak power by about a factor of 4 at the highest power level shown in Fig. 3, but achieves only 50% of the unbloomed peak intensity. This result is somewhat unexpected because of the different geometries in the two experiments. The gas cell is a distributed disturbance and extends from the near field to the focus of the beam. The static liquid cell was very thin compared to the beam confocal parameter and was placed in the near field of the transmitter.

The cases of greatest practical interest are those which simulate forced convection-dominated blooming. A series of tests were made using the parameters shown in Table 1. The observed beam profiles through the cell are shown in Figs. 4 and 5. The profiles in Fig. 4 are A-scope presentations which show the entire beam in profile; the main lobe as well as the sidelobes can be seen. Note that the vertical scale is logarithm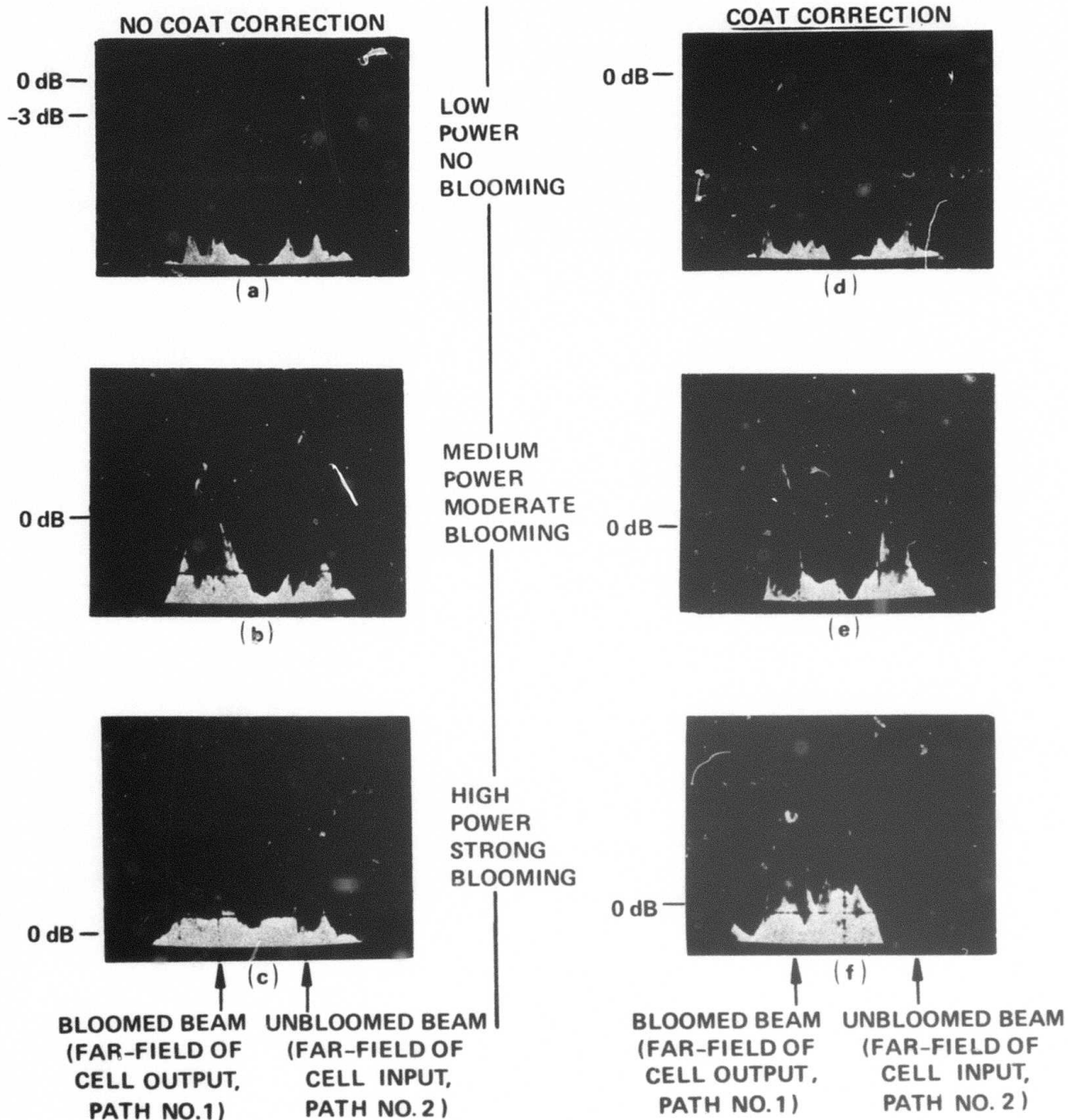ic. The photographs in Fig. 5 are black-and-white photographs from a level-quantized color display[3] with 1.5 dB per color level and correspond to the profiles shown in Fig. 4.

There are three principal features of these data. First, the expected crescent-shaped beam distortion is observed in Fig. 5(c) and the beam is shifted into the wind as shown in Figs. 4(c) and 5(c). Note that the crescent is also shifted toward the top of the photograph in Fig. 5(c); the possible significance of this is discussed below. Second, when the COAT correction is applied, the beam maximum is maintained on the boresight

Table 1. Single Glint Thermal Blooming Parameters

$V$ = Transverse wind velocity = 6.4 cm/sec

$aL$ = Absorption coefficient = 1.22 (cell transmission = 30%)

$D_T$ = Beam diameter at cell input = 0.26 cm

$D_f$ = Beam diameter (diffraction-limited) at cell output (beam focus) = 0.022 cm

T1580

**NO COAT CORRECTION**

3751—35R1

3751—35R1

**COAT CORRECTED**
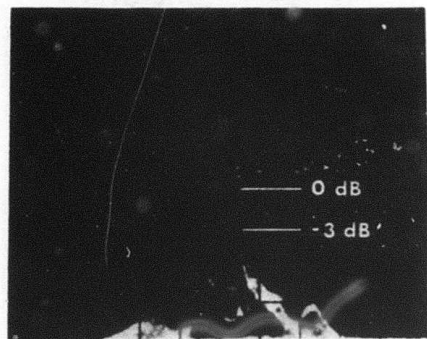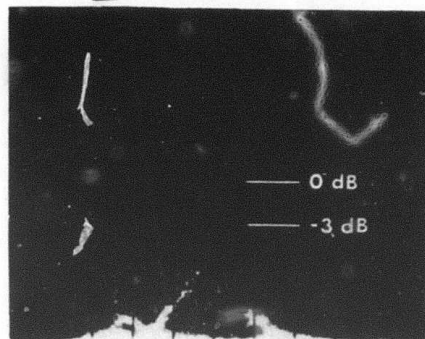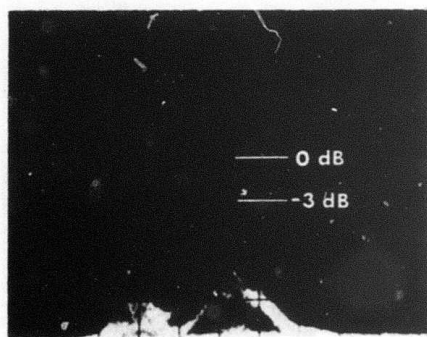


LOW
POWER
P = 12 mW
NO
BLOOMING

(a)

(d)

MEDIUM
POWER
P = 24 mW
MODERATE
BLOOMING

(b)

(e)

HIGH
POWER
P = 68 mW
STRONG
BLOOMING

(c)

BORESIGHT AXIS

(f)
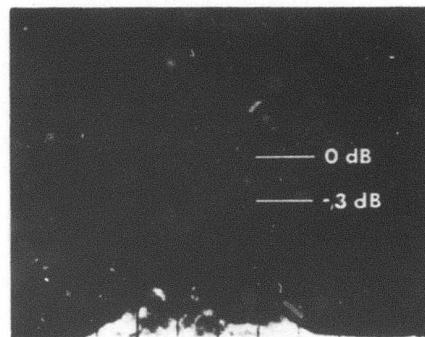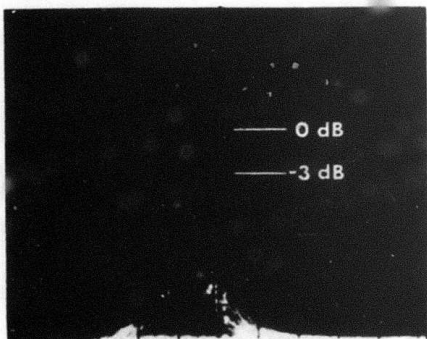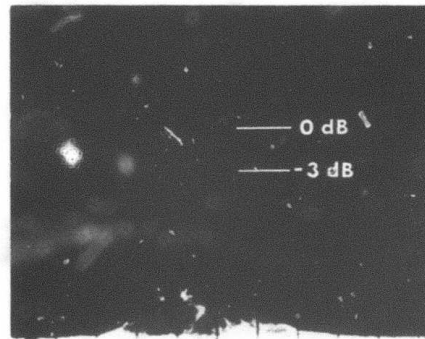
BORESIGHT AXIS (GLINT LOCATION)

3751—35

Fig. 4.  Forced convection blooming:  far field beam profiles
of bloomed beam.  (a) through (c) - No COAT cor-
rection.  (d) through (f) - with COAT correction.
Note the logarithmic scale.

17

**NO COAT CORRECTION**

**COAT CORRECTED**

LOW
POWER
P = 12 mW
NO
BLOOMING

(a)

(d)

MEDIUM
POWER
P = 24 mW
MODERATE
BLOOMING

(b)

(e)

HIGH
POWER
P = 68 mW
STRONG
BLOOMING

(c)

**BORESIGHT AXIS**

(f)

**BORESIGHT AXIS**
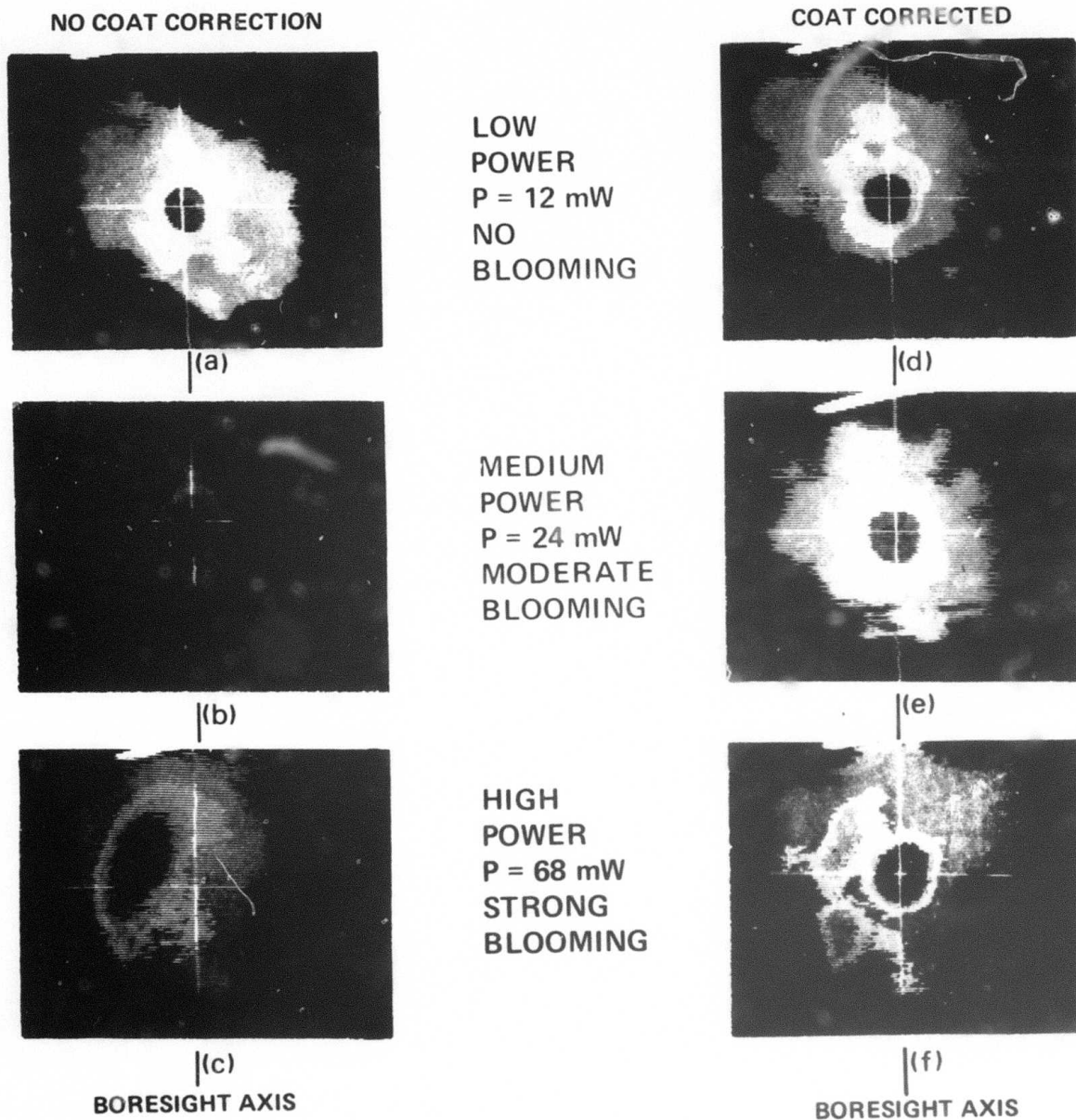
Fig. 5. Forced convection blooming: target intensity patterns
corresponding to profiles in Fig. 4. Each shading
level differs from the adjacent one by 1.5 dB.

axis where the glint is located. Finally, comparing Figs. 4(b) to 4(e) and Figs. 4(c) to 4(f) indicates no apparent improvement in peak intensity when the COAT correction is applied.

This last observation is quantified in Fig. 6. Also shown in Fig. 6 is the power through an aperture the width of which equals the full-width at half-maximum of the unbloomed beam. A small improvement in this "power in a bucket" is seen with COAT correction at the highest input power. Both the peak irradiance, $I_p$, and the aperture power, $P_a$, are the maximum in the beam, no matter where it occurred. For the COAT-corrected cases, the beam was also manually steered (usually only horizontally) to maximize
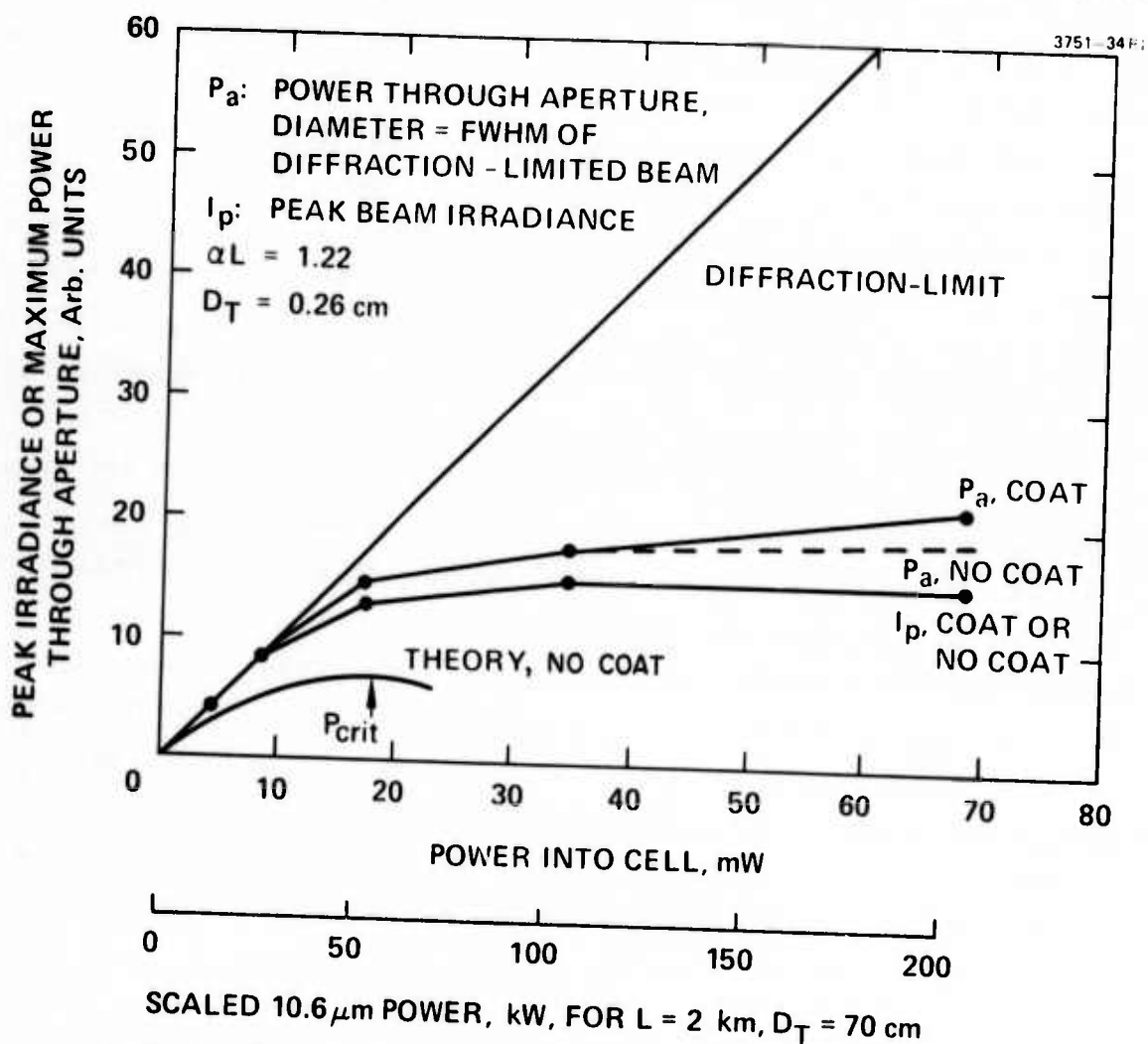


Fig. 6. Quantitative blooming data with and without COAT correction. The peak irradiance is the maximum in the beam no matter where it occurs. The power through the aperture, $P_a$, is also the maximum no matter where it occurs.

19

$I_p$ and $P_a$. Without this steering, the COAT-corrected curves would fall below the "NO COAT" curves. There is thus a significant wedge in the blooming distortion, which the segmented aperture phase correction in our system cannot adequately remove. An automatic pointing control (discussed in Section D) thus appears to be very desirable for coping with thermal blooming.

The data in Fig. 6 has two other noteworthy features. First, the amount of blooming calculated using the Naval Ordnance Laboratories (NOL) propagation code is indicated by the curve marked "theory". When scaled to a 2 km path and a 70 cm diameter transmitter at 10.6 μm, the 10.6 μm transmitter power is given by the scale at the bottom of the figure. The feature to notice is that the observed power reduction caused by blooming is only half that predicted by theory.

The second important feature of the experimental data is the absence of a well-defined "critical power" ($P_{crit}$ in Fig. 6) above which the target irradiance decreases with increasing transmitter power. Although not the same numerically, the experimental and theoretical curves in Fig. 6 have nearly the same shape up to $P_{crit}$, but above this power the experimental curves flatten out or saturate. This behavior has been observed by others in a different type of experiment[4] where the saturation was attributed to natural convection (buoyancy). The shift of the "crescent" in Fig. 5(c) is also indicative of convection effects (the top of the photographs in Fig. 5 correspond to the lower edge of the actual beam). This shift, the "saturation" of the observed blooming, and the lower than theoretical blooming levels lead us to conclude that buoyancy effects were present in our experiments. The easiest solution to the buoyancy problem is to mount the cell so that the laser beam propagates vertically. This is easily done and the resulting setup is shown in Fig. 7.

There is one other possible problem in our experiment. The ratio of the diffusion time across the beam to the forced convection transfer time is given by the Peclet number defined as

$$P_e = \frac{V r_o}{D} \tag{1}$$

20
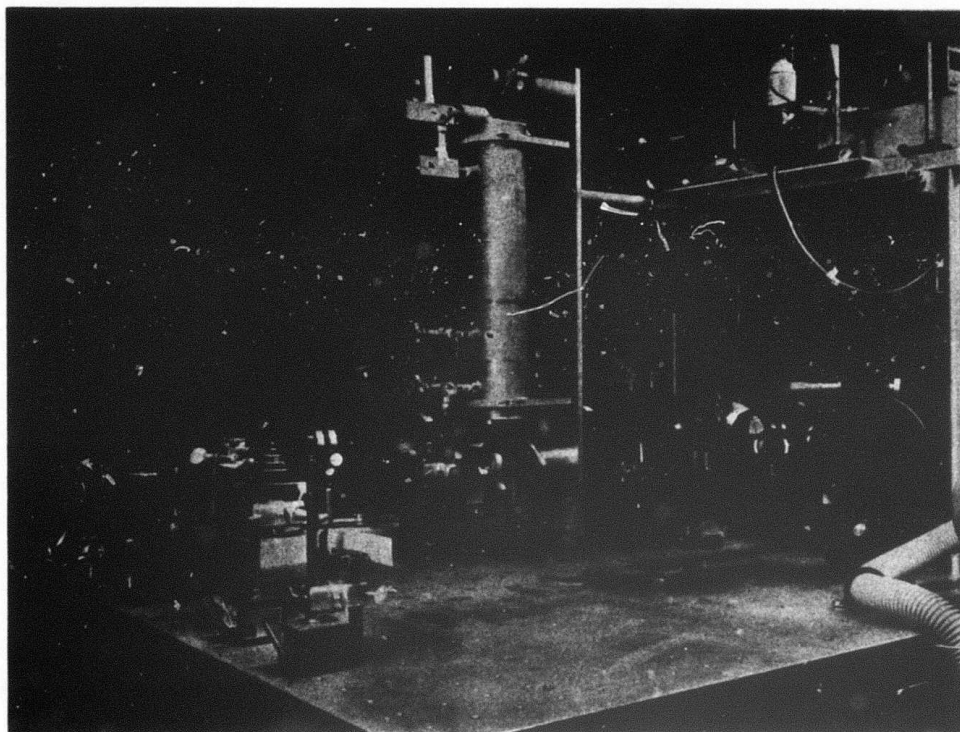
Fig. 7.  Modified gas cell arrangement.  The gas cell is mounted
vertically to minimize natural convection effects.

where V is the transverse wind velocity, $r_o$ is the beam radius, and D is the
medium diffusivity.  For convection-dominated heat transfer, $P_e \gg 1$.
Taking $P_e \geq 5$ as sufficient, and noting that $D = 0.054$ cm$^2$/sec for Xe at
atmospheric pressure, we find that in our experiment we must satisfy the
condition

$$Vr_o \geq 0.27 \quad . \tag{2}$$

The parameters in Table 1 are appropriate for the data shown in
Figs. 4 through 6, so $Vr_o = 0.83$ at the cell input; the condition in eq. (2) is
satisfied.  At the beam focus, however, $r_o = 0.011$ cm (diffraction-limited
spot) and $Vr_o = 0.070$, a factor of 3.8 too low if eq. (2) is to be satisfied.
We thus need to increase the wind speed by about a factor of 4 to ensure the

21

proper heat transfer characteristics along the entire beam path. Unfortunately, we will not be able to produce significant blooming with such wind velocities because of limited laser power (the blooming strength varies as $V^{-1}$). We may be able to increase V by a factor of 2 or 3, however, which should improve the agreement between theory and experiment.

The system convergence time was measured for the no wind case at the three blooming levels shown in Fig. 3. A convergence time of 1.5 to 2.0 msec was observed at all three power levels; the blooming appears to have no effect on the system convergence time.

### 2. Liquid Cell

The previous report[2] presented results of blooming studies which used a thin static liquid cell. The observed COAT performance was similar to the data in Fig. 3. We recently tested, on the HRL IR&D program, a flowing liquid cell which uses methanol with a small amount of iodine dissolved in it. The cell is 20 cm long and was used in the same position as the 50 cm gas cell as indicated in Fig. 2; the beam focus occurred near the cell output.

The advantage of the liquid cell is that significantly more blooming can be produced for a given optical input power to the cell; it is thus somewhat easier to eliminate convection problems. A disadvantage of the liquid cell is that the difference in fluid dynamics between an incompressible liquid and a compressible gas makes it more difficult to interpret the results in terms of a scaled-up atmospheric experiment.

We have had a limited amount of time to observe the COAT system performance with this cell. Qualitatively, the performance is the same as with the gas cell: some blooming compensation, but not as much as hoped for. We plan to obtain more quantitative data during the next quarter.

B.    Thermal Blooming – Computer Simulation Studies[*]

Although most of the computer code development is now complete, there are several subprograms which are still being implemented. These include finite extent, moving glints for the target simulator and auto focusing and auto tracking simulators. The linear and nonlinear propagation simulators and the multidither servo simulators are essentially complete, and mirror simulations have been developed for 37, 57, and 97 actuator deformable and segmented mirrors. A remaining problem is to combine all of these subprograms into an efficient master adaptive optical system simulator. This integration work has now started with the acquisition of remote-terminal batch processing lines to the computer facilities at the Lawrence Berkeley Laboratory and at the University of Southern California.

### 1.    Computational Results

To date, we have investigated COAT system performance only with a phase conjugate correction algorithm for economy in computer time. The correction mirror is "ideal" in that the number of actuators equals the number of calculational mesh points. The target is a single, stationary Gaussian glint, and turbulence as well as thermal blooming effects have been studied separately and together. Both pulsed and cw propagation cases have been studied. In this report, however, we discuss only cw cases. Figures 8 and 9 show the effects of turbulence and blooming on a 70 cm diameter beam focused at a distance of 2 km. Both figures are for stationary beams (no slewing) with no COAT correction. Figure 8 is computed for $\lambda = 3.8\ \mu$m and shows the dominance of turbulence effects at this wavelength. With no turbulence ($C_N^2 = 0$), the maximum flux on target is 53 kW/cm$^2$ at a critical transmitter power of 100 kW. With only moderate turbulence, the target flux at 100 kW transmitted drops by a factor of 4.1 to 13 kW/cm$^2$.

The 10.6 $\mu$m case in Fig. 9 shows the dominance of thermal blooming at this wavelength (the atmospheric absorption is 10 times stronger than at

---

[*]All of the computer simulation results presented in this report were obtained as part of DARPA/NOL Contract No. N60921-74-C-0249. The results have been previously discussed in other presentations.[5,6] They are presented here because of the relevance of the results to the experimental work accomplished on this contract.

23

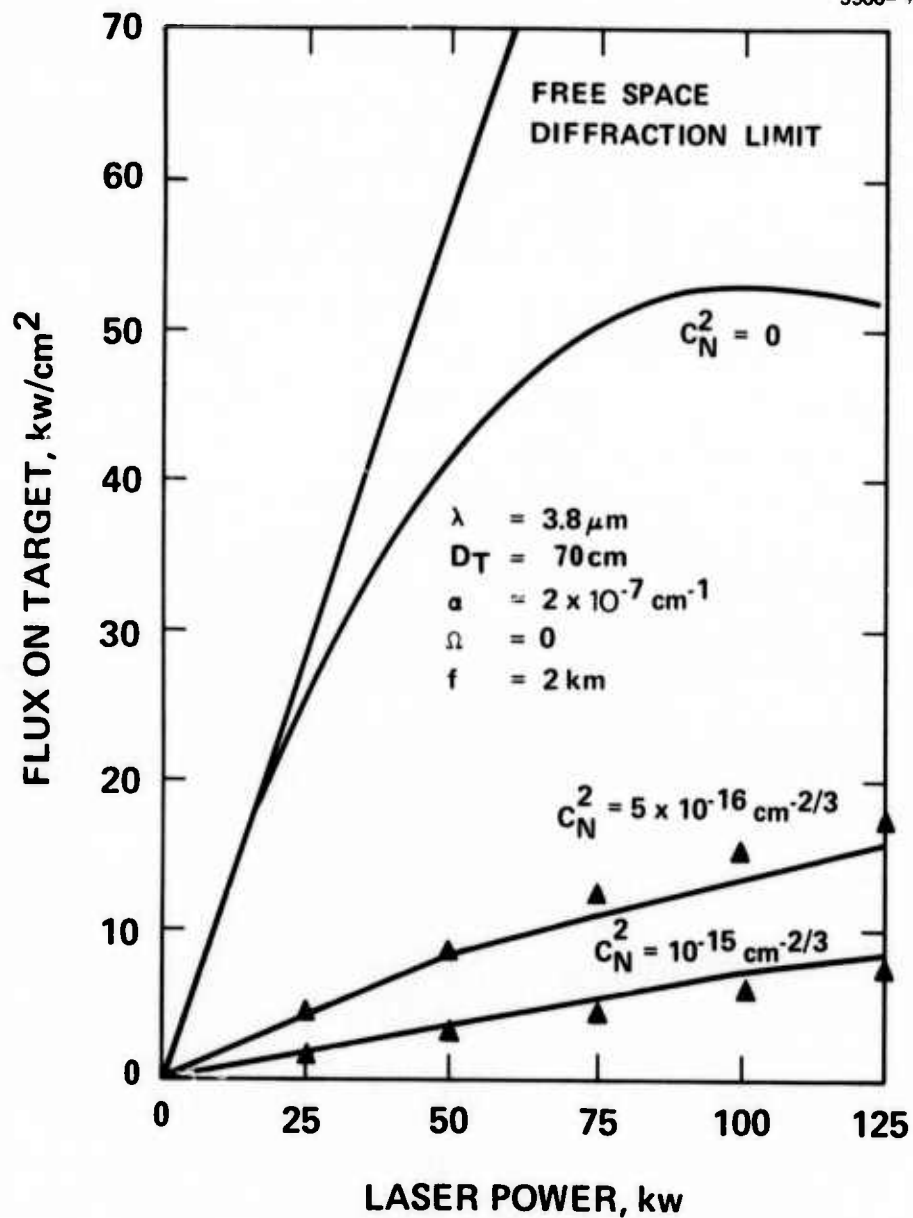
Fig. 8. Turbulence and thermal blooming effects at 3.8 μm with no beam slewing ($\Omega = 0$) and no COAT correction. The triangular points are found from a mean square combination of turbulence and blooming when considered separately (eq. (5)). Note the dominance of turbulence effects.

Fig. 9. Turbulence and thermal blooming effects at 10.6 μm with no beam slewing ( = 0) and no COAT correction. The triangular points are found from a mean square combination of turbulence and blooming when considered separately (eq. (5)). Note the dominance of blooming effects (compare vertical scale to Fig. 8).
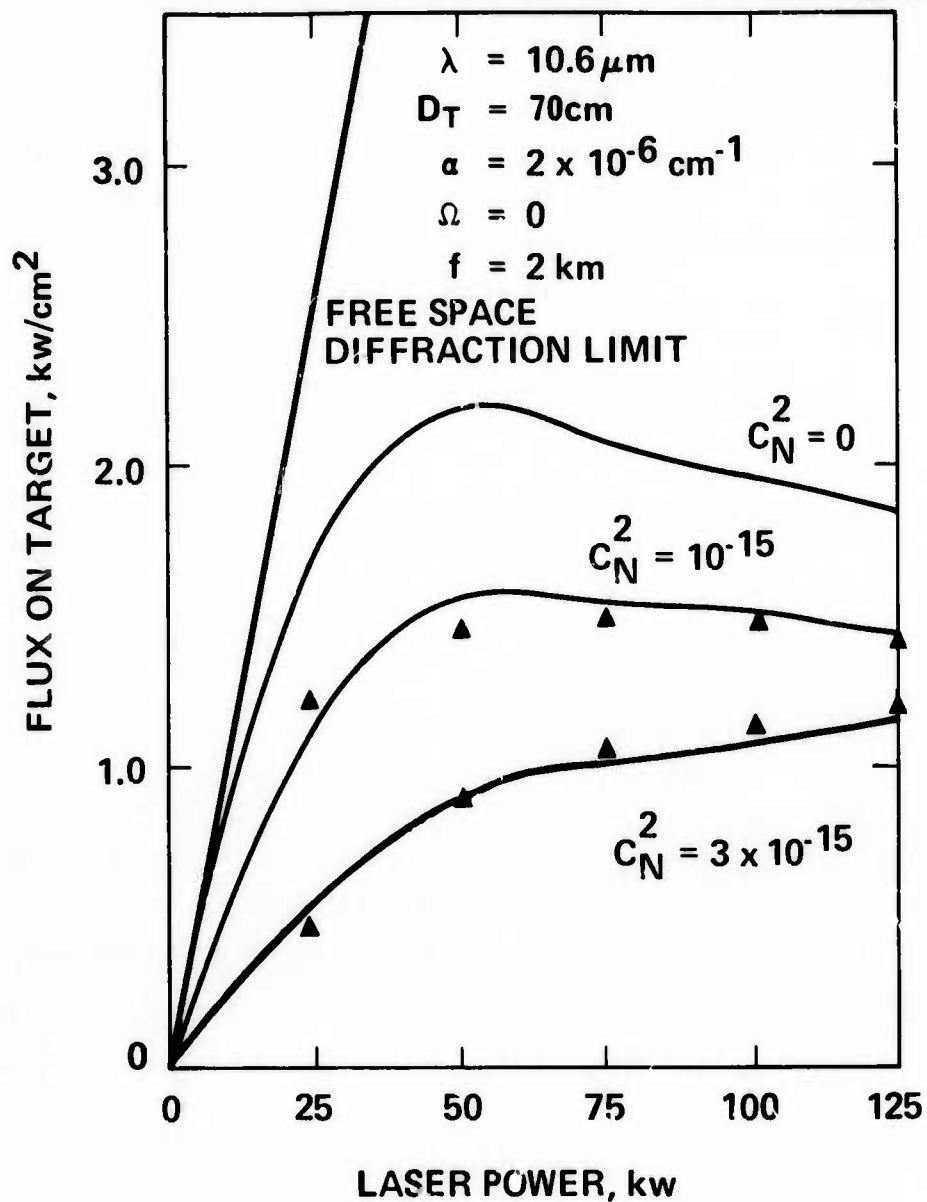
3.8 μm). With no turbulence, the maximum flux on target is only 2.2 kW/cm$^2$ at $P_{crit}$ = 54 kW. The triangular points in Figs. 8 and 9 are found from a mean square summation of the effects of turbulence and blooming considered separately. That is, for each type of distortion, we can define an effective distortion-induced divergence angle $\theta_B$ or $\theta_T$ such that the peak intensity on the target is given by

$$\frac{I_{peak}}{I_o} = \frac{1}{1 + \left(\frac{\theta_B}{\theta_o}\right)^2} \quad , \quad \text{blooming only} \tag{3}$$

or

$$\frac{I_{peak}}{I_o} = \frac{1}{1 + \left(\frac{\theta_T}{\theta_o}\right)^2} \quad , \quad \text{turbulence only} \tag{4}$$

where $\theta_o$ is the divergence angle for free space which produces an intensity $I_o$. An identical formulation was used in the previous report[2] to analyze blooming in a liquid cell. The combined effect of turbulence and blooming is then approximated by

$$\frac{I_{net}}{I_o} = \frac{1}{1 + \left(\frac{\theta_B}{\theta_o}\right)^2 + \left(\frac{\theta_T}{\theta_o}\right)^2} \quad . \tag{5}$$

As can be seen from the figures, this method gives results which are very close to the calculation which considers the two effects simultaneously.

We have previously demonstrated both experimentally[2] and through computer simulation[5] that a COAT system can remove 90 to 95% of turbulence distortions. COAT correction for thermal blooming in the presence of beam slewing has been studied with two scenarios. First, using a phase conjugate algorithm, the correction is applied to an infinite Gaussian beam across the entire computational screen at every mesh point. This

corresponds to a system with a very large, perfectly deformable mirror with effectively an infinite number of actuators. The results of this type of calculation for $\lambda = 10.6$ μm are shown in Fig. 10 for a beam slew rate of 20 mrad/sec. The COAT correction increases $P_{crit}$ by a factor of 2, and increases the maximum flux on target by a factor of 2.9. Note also the substantial increase in target irradiance for a slewed beam over that for a stationary beam (Fig. 9).

The more realistic case, however, is for a truncated Gaussian beam. Figure 11 gives the results at 10.6 μm for a Gaussian beam truncated so that 90% of the original beam energy is transmitted. Again, phase conjugate correction is used but only over the finite transmitter beam. The first thing to notice is that the truncation reduces the diffraction-limited peak intensity by a factor of 2 from the infinite Gaussian case. Second, in the absence of turbulence, the COAT correction has almost no effect no $P_{crit}$ and increases the maximum target intensity by only 15%. Since this result is consistent
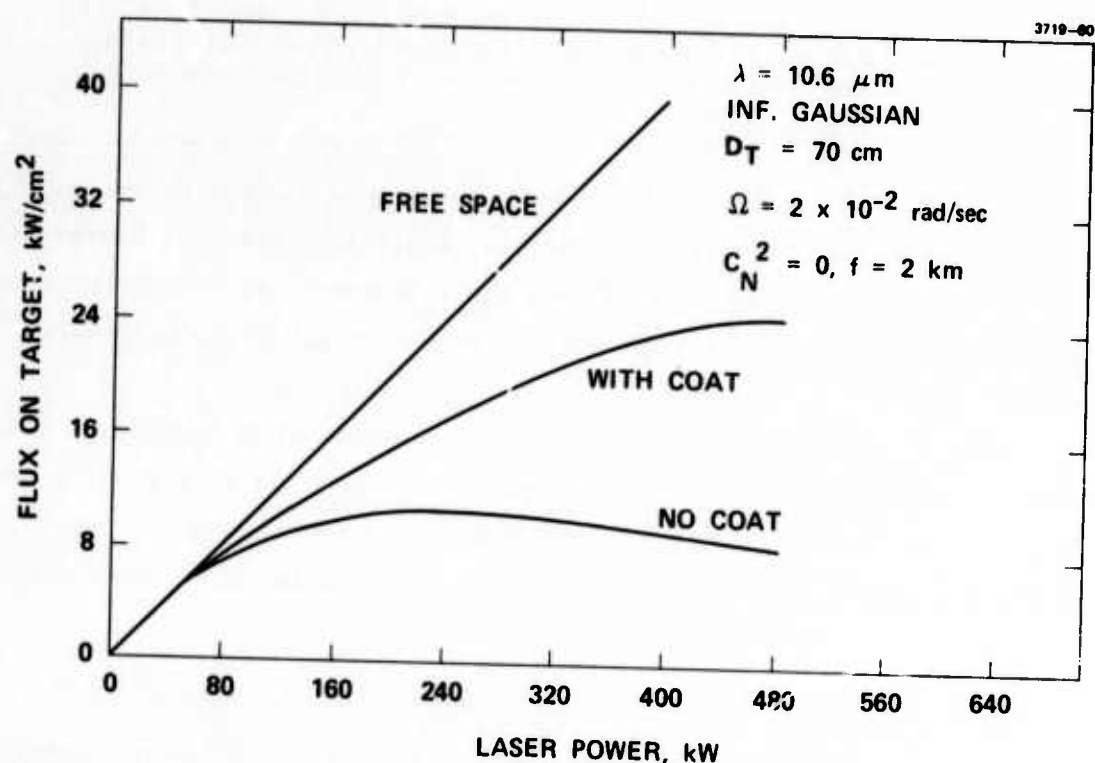


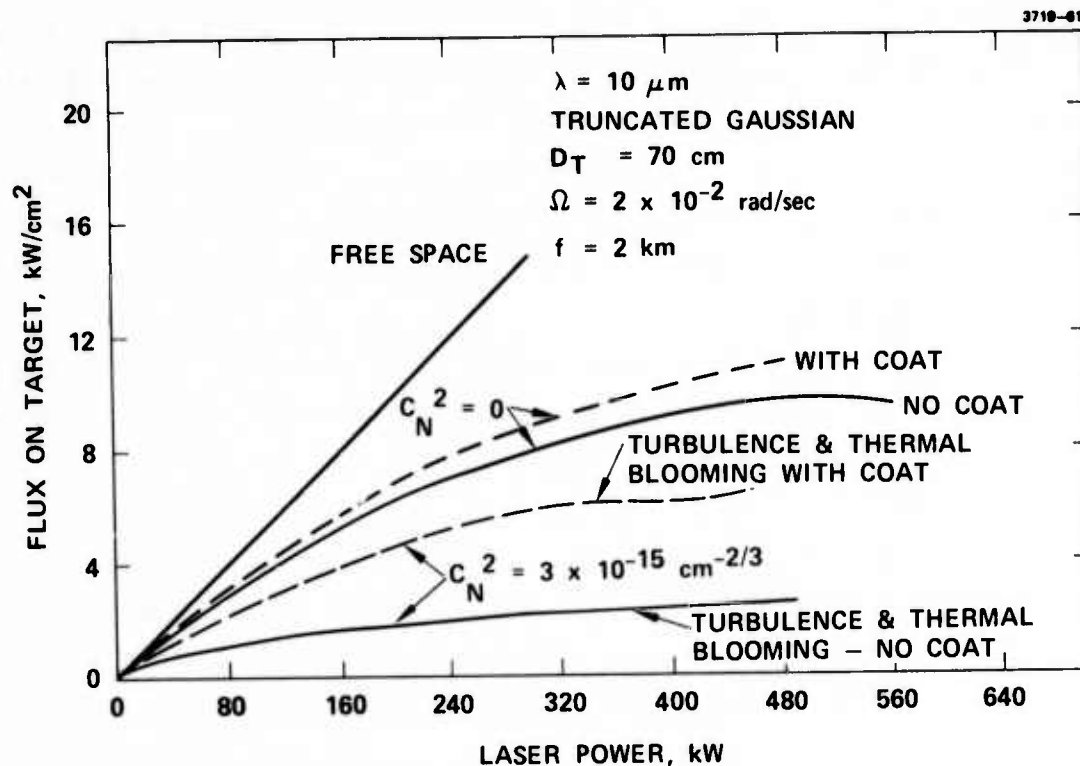Fig. 10. Phase conjugate COAT correction for thermal blooming at 10.6 μm for an "infinite" slewed beam as explained in the text.

27

Fig. 11. Phase conjugate COAT correction for thermal blooming at 10.6 μm for a truncated Gaussian beam with beam slewing. Cases with and without turbulence are shown.

with our multidither experimental results, we have no reason to suspect that the use of a multidither algorithm in the simulation will give any better COAT correction. With both blooming and turbulence present, substantially more correction is observed; COAT correction removes most of the turbulence distortions.

Figure 12 shows the effect of COAT correction at 3.8 μm for a truncated Gaussian beam. The transmitter diameter and slew rate are the same as in Fig. 11, but the focal distance and turbulence are different. Again, most of the turbulence distortions are removed, but little correction for thermal blooming is observed.

2. Discussion

Although the results presented above are still somewhat preliminary, it appears reasonable to draw two tentative conclusions. First, a COAT system which provides phase control at the transmitter aperture can
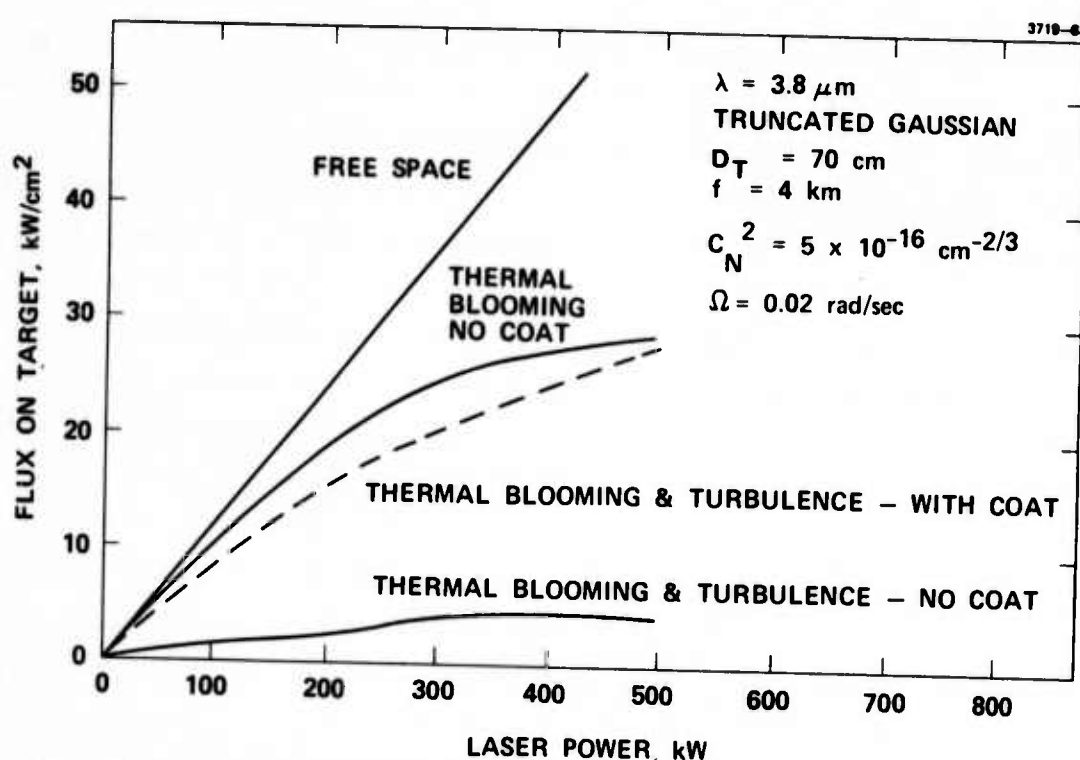
Fig. 12.   Phase conjugate COAT correction for thermal blooming
and turbulence at 3.8 μm for a truncated Gaussian
beam with beam slewing.

provide some compensation for thermal blooming but the amount of correction is small.   The apparent factor of 4 correction seen in Fig. 3 (no wind) may be caused by turbulence-like effects produced by strong convection currents set up in the gas (observe the greatly diffused beam in Fig. 3(c)). The COAT system may just be removing the turbulence distortions.

We do not yet fully understand why COAT correction when applied to an "infinite" beam is so much better than when it is used with a truncated beam.    We think, however, that it is in part caused by the fact that the distortions associated with the fields outside the truncation circle are more easily corrected by a phase conjugate COAT system than those inside this region, because the degree of distortion decreases as the distance from beam center increases; i.e., the fields near the beam center pass through the most severely distorted portions of the medium.   We plan to explore this phenomenon further during the next two quarters.

The second conclusion based on this early work is that automatic pointing and tracking is important in optimizing target irradiance in the presence of thermal blooming.   This conclusion is based on our qualitative

29

experimental observation that it was necessary to steer the beam to maximize the irradiance on a single glint after the COAT phase control had converged to its maximum level. That is, part of the blooming distortion is an effective wedge which our stepwise aperture phase control cannot remove (a deformable mirror would automatically do so, however). In effect, without any pointing correction, the COAT phase control maximizes the target irradiance, but on an "off-axis" glint; the pointing correction then removes the tilt component of the distortion. More detailed data to support this conclusion will be available after we have completed the addition of multidither pointing and focus controls to the RADC/COAT system.

It is worth noting that our observations of little COAT compensation for blooming for truncated beams do not agree with studies, both experimental and theoretical, made at Lincoln Laboratories.[7,8] This work considered the introduction of optimized amounts of classical aberrations (tilt, focus, astigmatism, coma, etc.) to overcome blooming. Theoretically,[8] factors of 2 to 4 improvement were seen. Experimentally,[7] using only astigmatism and refocus, a factor of 2 increase in target irradiance was observed for $P \approx 1.5\ P_{crit}$.

This discrepancy with our work suggests two things: (1) We have some hidden error in both our experiment and simulation, or (2) we have not yet optimized the correction scheme for thermal blooming. We feel that the second item is the more likely explanation. The Lincoln Laboratories theoretical results were obtained using a predictive scheme based on the computed phase error across a bloomed beam. The various aberrations through fifth order were then fitted to this error and applied to the transmitted beam. Experimentally, the amount of astigmatism was varied until maximum target irradiance was achieved and then a small refocus correction was made. Both of these procedures can be considered equivalent to a slow, large amplitude dither algorithm which evaluates the effect of a correction before deciding on the next step. It may be that the multidimensional correction space for blooming has one or more local maxima which are not the global optimum. A "slow," high-amplitude correction scheme may be able to converge on the global optimum while the fast, low-amplitude multidither (or phase conjugate) technique hangs up on one of the local maxima.

This explanation is, of course, very speculative and needs much more study. We hope to address, in future work, the problem of identifying other correction algorithms for blooming compensation as well as for other applications.

## C. Complex Target Studies

We are just starting to investigate the effects of moving multiple glint or diffuse targets on the operation of multidither COAT systems. We have looked briefly at two-glint and multiple-glint scotchlite targets, where the glints are not resolved by the transmitter. Diffuse targets made of curved plastic or curved scotchlite have also been observed. These diffuse targets were usually cylindrical in shape and larger than the formed array beamwidth. No blooming or turbulence has been introduced in any of our tests to date.

One of the important parameters in this target study is ratio of the effective receiver resolution to the transmitter resolution. This ratio can be expressed as

$$\gamma_{RT} = \frac{R_T}{R_R} \times \frac{D_R}{D_T} \tag{6}$$

where $R_T(R_R)$ is the range from the target to the transmitter (receiver) and $D_T(D_R)$ is the largest dimension of the transmitter (receiver). As $\gamma_{RT}$ approaches unity, speckle patterns from complex, moving targets may cause amplitude modulations in the COAT receiver.[9] If these modulations have significant frequency components at a dither frequency, that servo channel might be disabled as long as the modulations persist.

Three types of targets have been investigated so far. The first target had two scotchlite glints located so both were within an array beamwidth and one was oscillated along the beam path at frequencies ranging from 10 Hz to 10 kHz. The maximum motion was varied from about 0.2 mm to 2 mm. The second target contained five small scotchlite glints all within an array beamwidth. The ensemble was given a low amplitude oscillatory motion about an axis perpendicular to the beam. The third target was a scotchlite cylinder rotated at various uncalibrated rates about an axis perpendicular to the beam.

31

Table 2. Preliminary Moving Complex Target Study Results

| $\gamma_{RT}$ \ Target | Two Glints, one moving | Multiple Glints, all moving | Extended, diffuse cylindrical target |
|---|---|---|---|
| 9 | No effect; good COAT performance | No effect | No effect |
| 0.33 | No effect; good COAT performance | No effect | COAT system breaks lock at slow rotation speeds |

T1599

The results of our measurements are summarized in Table 2 for two different values of $\gamma_{RT}$. For $\gamma_{RT}$ = 9, there is significant averaging over the receiver aperture and, as expected, no target effects were observed with any of the targets; the COAT system maintained lock on the moving targets just as well as on a single stationary glint. One qualification is necessary, however. Even when the cylindrical target was stationary, the beam formed by the COAT system tended to jump around a little because of the large effective glint area; the glint size is the same size as or larger than the formed array beamwidth. This type of behavior has also been observed on a 100 m outdoor range with this kind of target.[3]

With the small value of $\gamma_{RT}$ = 0.33, there was barely enough signal-to-noise (S/N) to maintain lock, even with a single stationary glint. Even with the low S/N, however, no target effects were observed except with the diffuse cylindrical target. In that case, the system did break lock when the cylinder rotated slowly; at faster rotation rates, the COAT system could maintain lock on the cylinder. We have not yet repeated this experiment in a quantitative fashion; in particular, we have not observed whether the system broke lock because of induced receiver modulations at the dither frequencies or because of the low S/N value. It is apparent, however, that a much more detailed study of these effects is required.

D.    Hardware Modifications

1.    Improved Noise Performance

Because of the low S/N values encountered in the target interaction studies, we are improving the preamplifier and line driver which

32

follows the COAT photomultiplier receiver. This modification should result in lower noise and dc drift in this part of the system, and hopefully will improve the overall loop S/N.

2. Active Point/Tracking and Focus Controls

Amendment No. 1 to this contract has provided $30K of additional funds to add multidither pointing/tracking and focus controls to both the RADC/COAT system and the NOL computer simulation. This work is now under way with the $30K split evenly between the hardware and the software modification tasks. Figure 13 shows schematically how the new controls will be implemented in the hardware during the next quarter. The additional signal conditioning in the pointing/focus loop allows us to optimize the performance of these channels without reducing the performance of the 18 phase control channels.

The new signal conditioning block elements shown in Fig. 14 are similar to those in the phase control loop. The multiplier automatic gain control (AGC) is the same one built and tested with the 18-element system. The dc amplifier preceding the AGC ensures operation within the dynamic range of the AGC and the following amplifier adjusts the overall loop gain. The phase reversal switch provides selection of the black hole tracking mode and the loop switch is for measuring convergence time. The three bandpass filters perform the dual function of dc rejection and reduction of noise bandwidth. The corner frequencies are chosen to be a factor of 10 above or below the nominal channel dither frequencies. These values ensure minimal phase shift at the dither frequencies and are consistent with a scaling of the phase control servo parameters.

The servo control parameters were chosen by appropriately scaling the optimized parameters in the 1 kHz response phase control system. The design goals for the new controls are 100 Hz response for the pointing and 10 Hz for the focus. There are two principal reasons for these choices. First, our turbulence range studies[3] have indicated that a 100 Hz pointing/ tracking response is desirable for turbulence compensation. Second, the desired order of convergence is (1) phase, (2) pointing, and (3) focus. Also, from a practical standpoint, it is difficult to implement these controls at much faster rates. The phase control parameters are thus scaled down by 10 for the pointing/tracking controls and by 100 for the focus control as shown in Table 3.
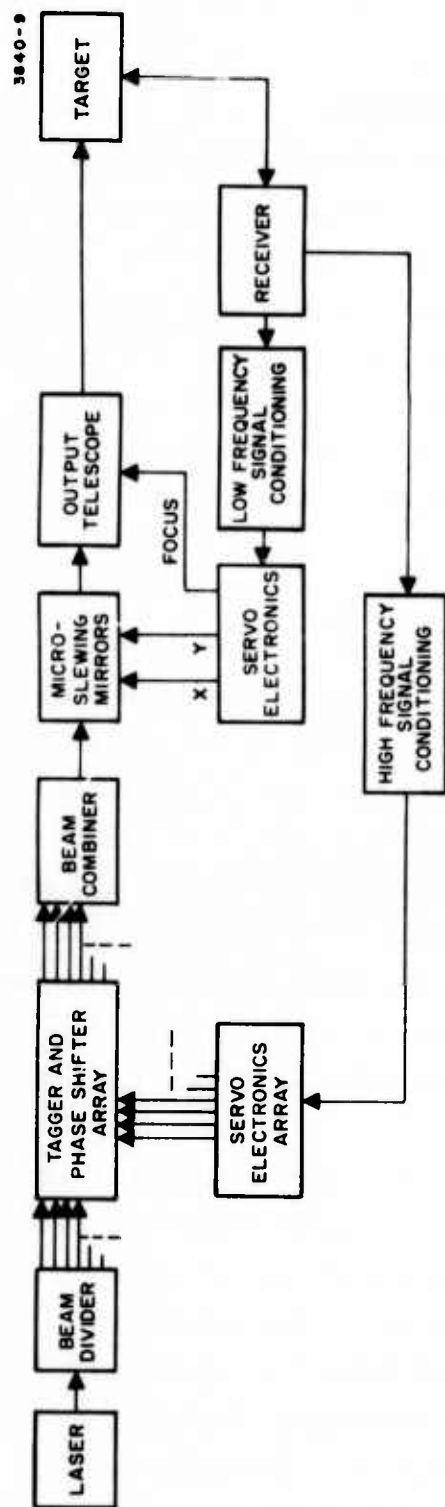
33

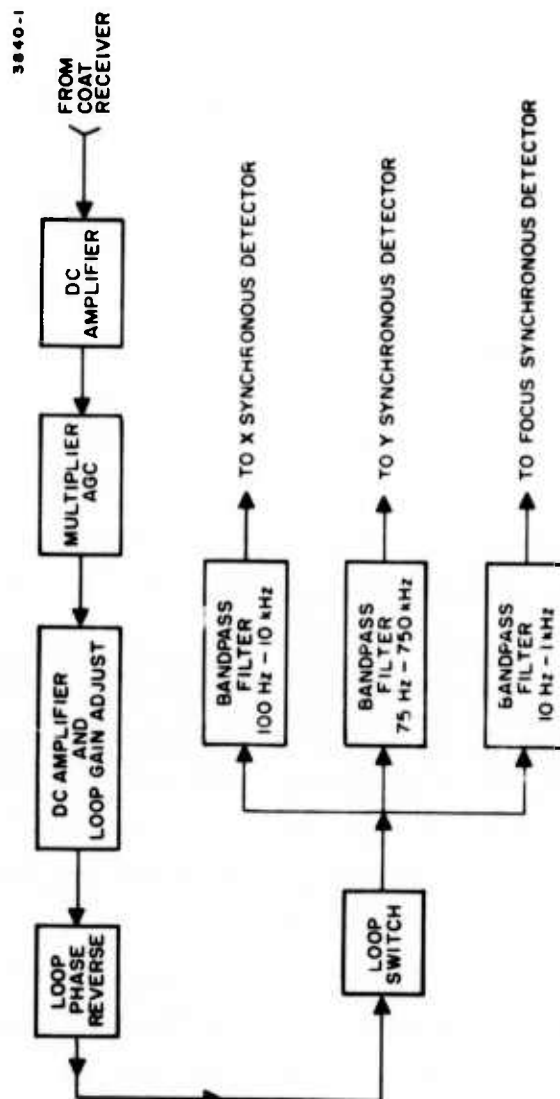Fig. 13. COAT system block diagram showing additional multidither servo loops for tracking and focus control.



Fig. 14. Pointing/focus control signal conditioning elements.

34

Table 3. Pointing/Tracking and Focus Servo Parameters

| Parameter | Phase Control | Pointing/Tracking | Focus |
|---|---|---|---|
| Frequency Response (nominal design goal) | 1 kHz | 100 Hz | 10 Hz |
| Dither frequencies loop | 8.2 kHz to 32 kHz ($\Delta f = 1.4$ kHz) | 1 kHz, 750 ($\Delta f = 250$ Hz) | 100 Hz |
| High-Pass filter | 1 corner at 1 kHz | 1 corner at 100 Hz | 1 corner at 10 Hz |
| Low-Pass filter | 1 corner at 10 Hz, 4 at 5 kHz | 1 corner at 1 Hz, 4 at 500 Hz | 1 corner at 0.1 Hz, 4 at 50 Hz |

T1600

The pointing control will be implemented using galvanometer mirror drivers and their companion amplifier/drivers built by General Scanning, Inc. The galvanometers are series 300 units with an unloaded fundamental resonance of 1400 Hz. The units will be placed along with the focus control mirror after the first reducing telescope in the laboratory optics (see Fig. 2) so that small mirrors can be used. With the pointing mirrors in this location, the dynamic range of the tracker will be limited by the optical system rather than by the galvanometer motion; at least ±3 element widths should be available. The objective here, however, is to demonstrate the usefulness of adaptive pointing control coupled with phase control for blooming and turbulence compensation rather than to make a wide dynamic range tracker.

The amplifier/drivers for the galvanometers are the RAX-100 units used previously in the RADC/COAT system for offset pointing studies. Because of the gain in these units, only a small dc gain will be necessary in the pointing low-pass filter loops shown in Fig. 15(a). The pointing control has the capability of separate dither frequencies on the x and y mirrors, but we intend to operate with the sine and cosine of 1 kHz unless some problem arises with the method. With sine/cosine operation, the pointing control is effectively a conical scan pointer/tracker.
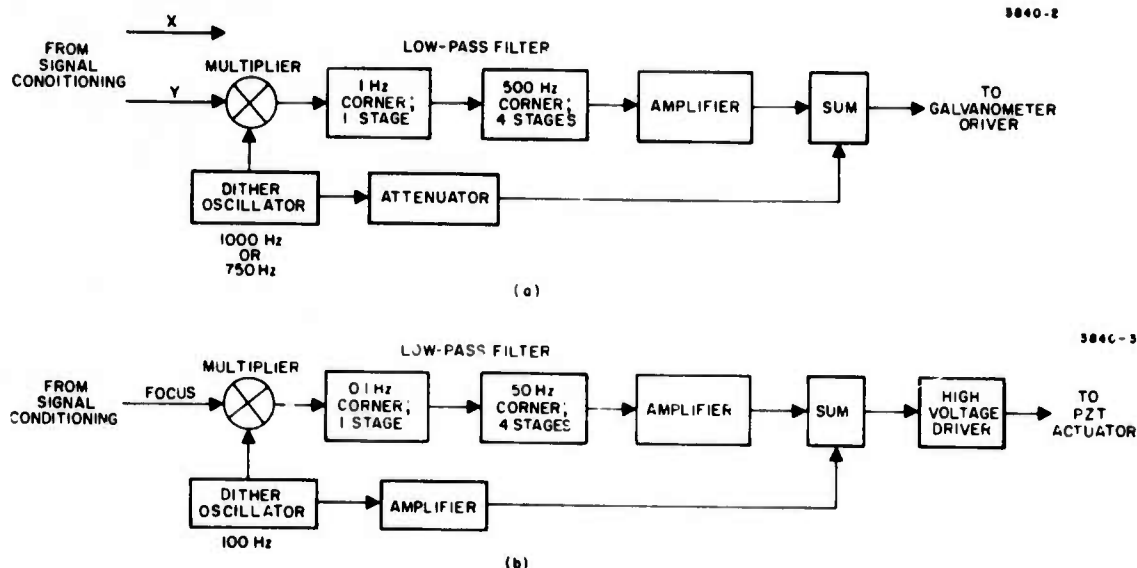
Fig. 15. Block diagram of servo control channels for
pointing and focus functions. (a) x or y
pointing channel, (b) focus channel.

The focus control channel shown in Fig. 15(b) is functionally similar
to the pointing control channel except that a 1000 V peak-to-peak amplifier is
required to drive the piezoelectric focus control actuator. The actuator is
a 2.25 in. long, 3/8 in. diameter, 0.0875 in. wall cylinder of PZT-5H.
The effective spring constant for this cylinder is $4.18 \times 10^5$ lb/in. The unit
when end mounted has an unloaded response of $S_u = 201$ V/$\mu$m. This actu-
ator is used to change the radius of curvature of a long-radius spherical
mirror as shown in Fig. 16. The mirror is actually flat before mounting,
but a preload and dc bias on the cylinder will be used to give it a slight out-
ward (convex) curvature. This allows the PZT actuator to work against the
spring of the mirror and eliminates the need for bonding the cylinder to the
mirror back surface.

Care must be taken to ensure that the mirror is not too stiff since the
effective loaded PZT response, $S_L$, is given by
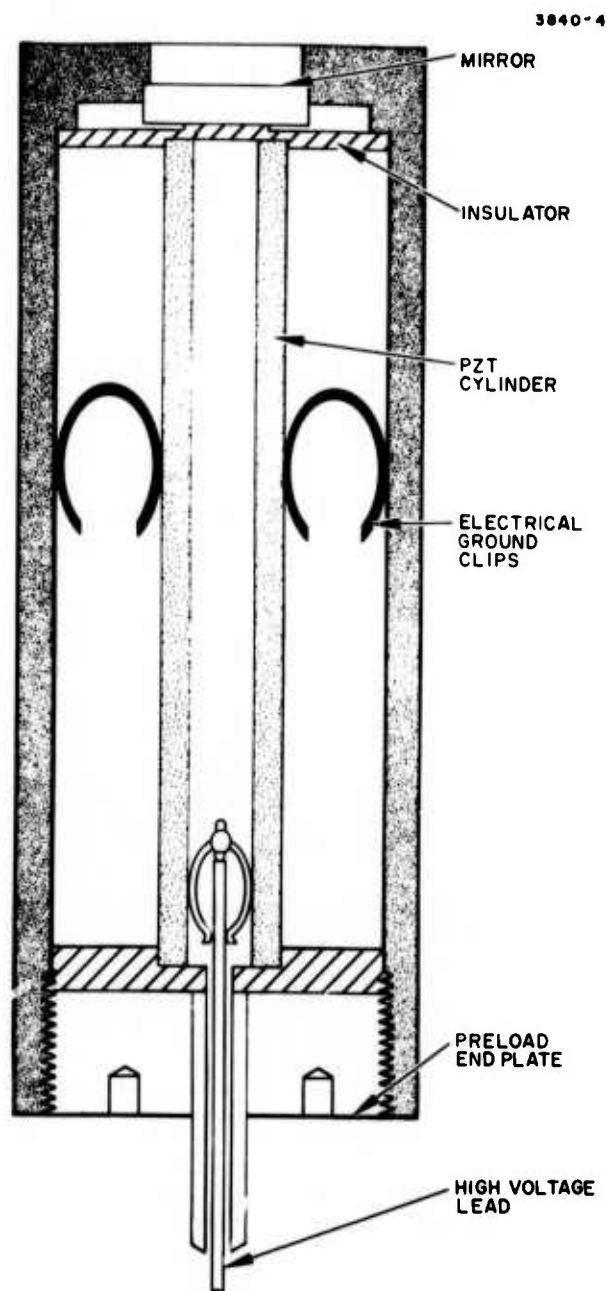
$$S_L = S_u \frac{K_c}{K_c + K_m} \tag{7}$$

3840-4



Fig. 16. Piezoelectrically-driven,
variable-radius spherical
mirror used for autofocus
control.

MIRROR

INSULATOR

PZT
CYLINDER

ELECTRICAL
GROUND
CLIPS

PRELOAD
END PLATE

HIGH VOLTAGE
LEAD

where $K_c$ and $K_m$ are the spring constants of the cylinder and mirror. The spring constant of an edge supported mirror with a uniform concentric annular load varies in the following manner:[11]

$$K_m \propto \frac{t^3}{d_o^2} \ g\left(\frac{d_m}{d_o}\right) \quad , \tag{8}$$

where $t$ is the mirror thickness, $d_m$ is its diameter, and $d_o$ is the radius of the concentric circular ring load. The function $g$ involves only the ratio $d_m/d_o$. For a constant $d_m/d_o$, Table 4 presents three examples of possible mirror designs for this actuator. Since we want $K_m \ll K_c$, only cases I and III should be considered ($K_c$ = 418,000 lb/in.) The dependence of the required mirror excursion on $d_m$ will then make the final choice.

The required excursions of the mirror actuator are found by considering an initially collimated Gaussian beam of diameter $D$ incident on a lens of focal length $f$ (the first lens marked $f_1$ in Fig. 2, for example). The beam Fresnel number is then defined as $F = f/D$. The divergence $\theta_i$ (wave front curvature $R$) of the input beam is then varied to move the focal plane by $\Delta Z$. The quantities $\theta_i$ and $R$ are related for small $\theta_i$ and large $R$ by

$$R = \frac{D}{2\theta_i} \quad . \tag{9}$$

Table 4.  Spring Constants for an Edge-Supported,
Concentric Ring-Loaded Glass Mirror

|  | I | II | III |
|---|---|---|---|
| Mirror Thickness, $t$ (cm) | 0.318 | 0.318 | 0.191 |
| Mirror Diameter, $d_m$ (cm) | 2.54 | 1.27 | 1.27 |
| Load Diameter, $d_o$ (cm) | 1.27 | 0.635 | 0.635 |
| Spring Constant, $K_m$ (lb/in.) | 120,950 | 483,800 | 104,500 |

T1601

38

For $\theta_i << 1/F$, it is easy to show that the change in $\theta_i$ required to produce a given $\Delta Z$ is

$$\Delta \theta_i = \frac{\Delta Z}{fF} \quad . \tag{10}$$

Now, consider an initially flat mirror of diameter $d_m$ which is clamped at its perimeter. A force applied to the center of this mirror will cause it to bow into an approximately spherical surface for small deflections. The center deflection required to produce a radius of curvature $R$ is

$$\delta = \frac{d_m^2}{8R} \quad . \tag{11}$$

Assuming $\theta_i \approx 0$ initially, $\Delta \theta_i \approx \theta_i$ and eqs. (7) to (9) can be combined to give

$$\delta = \frac{d_m^2 \Delta Z}{4f^2} \quad . \tag{12}$$

The fractional change in intensity of a Gaussian beam near its focus is given by

$$a = \frac{I_o - I(z)}{I_o} = 1 - \frac{w_o^2}{w^2} \tag{13}$$

where

$$w^2 = w_o^2 \left[ 1 + \left( \frac{Z}{Z_R} \right)^2 \right]^{1/2} \tag{14}$$

and $I_o$ is the intensity at the focus ($Z = 0$). The minimum spot radius is $w_o$ and $Z_R = \pi w_o^2 / \lambda$. For a given $a$, the required distance $Z = \Delta Z$ from the focus is

$$\Delta Z = Z_R \left( \frac{a}{1 - a} \right)^{1/2} \quad . \tag{15}$$

Since $w_o$ occurs at the focus of a lens, for diffraction-limited performance $w_o = 2\lambda F/\pi$. Using this and the definition of $Z_R$ in eq. (13) gives

$$\Delta Z = \frac{4\lambda F^2}{\pi} \left(\frac{a}{1-a}\right)^{1/2} \quad . \tag{16}$$

Putting eq. (14) in eq. (10) gives

$$\delta = \frac{\lambda}{\pi} \left(\frac{d_m}{D}\right)^2 \left(\frac{a}{1-a}\right)^{1/2} \quad . \tag{17}$$

It is interesting that the result in eq. (17) is independent of the lens focal length, depending only on the input beam and mirror diameters. For a given $a$, $d_m$ should be as small as possible to minimize $\delta$ and thus the required drive voltage, $V$ ($\delta = V S_u$). This requirement selects case III in Table 4 as the best mirror design. Much smaller mirror diameters than 0.5 in. are not practical, because the mirror becomes too thin and because of the beam size incident on the mirror.

For dithering, $a = 0.02$ is sufficient. For the mirror placed after the first telescope in the setup shown in Fig.2, $D = 0.46$ cm and $f = 91$ cm so that $F = 198$. Use of eq. (15) for $d_m = 1.27$ cm gives $\delta = 0.17$ μm for a 2% peak amplitude change dither. The loaded response of the PZT driver is 250 V/μm so a voltage of 85 V peak-to-peak is required for the dither. The maximum peak driver voltage of 500 V (1000 V peak-to-peak) provides $\delta = 2.0$ μm corresponding to a factor of 3.85 change in the intensity in the lens focal plane. This change is produced by a peak motion of the focal plane of 4.1 cm or 4.5% of the 91 cm focal distance. These values should be sufficient to observe any effect of defocusing on blooming correction.

### 3. Flowing Gas Cell

The present design for the gas cell and wind generation mechanism[2,3] was chosen because it presented the fewest risks for successful implementation. The design has performed as expected, but it does suffer from three disadvantages; the wind direction reverses periodically, the beam must be blocked 50% of the time to ensure that the wind velocity is nearly uniform, and the optical arrangement does not allow the blooming

40

medium to fill the entire region between the focal plane and the transmitter aperture. The first two problems have so far been only inconveniences, but may become intolerable with moving targets. The third feature is not serious, since the focal plane is in the blooming medium as is 60% of the transmitter to focal-plane path. It does constitite a discrepancy between the computer simulation and the experiment, however, and will take on greater importance with slewed beams.

In order to correct these deficiencies, we have designed and are now building a flowing gas cell. The design is shown schematically in Fig. 17. The cell will be mounted so the optical path is vertical to minimize buoyancy effects. Sintered nickel baffles are used to produce turbulence-free laminar flow across the optical path. The wind velocity is varied by a speed control on the centrifugal fan which has a capability of producing flow rates of 10 cfm against a pressure drop of 50 in. of water. This is more than sifficient for our application. The wind velocity will be measured with a calibrated hotwire anemometer built by Thermo-Systems, Inc. We plan to complete construction, testing, and calibration of this cell during the next quarter.

4. Turbulence Generation

Generating artificial turbulence in the laboratory is not difficult, but doing it in a calibrated fashion is. We have decided to use a single phase screen which will be placed just ahead of the lens which focuses through the gas cell. We have two designs for this screen indicated in Fig. 18, each of which has its good and bad features.

The phase screen shown in Fig. 18(a) is fabricated by sputtering patches of $SiO_2$ onto a fused quartz plate through a mask. The mask is a thin metal plate with holes of four different sizes drilled in it in a randomized fashion. The hole diameters are arbitrarily chosen as 6, 4, 3, and 2 times an element size, so that the average "correlation distance" will be larger than the element diameter but smaller than the full transmit aperture. Two or three evaporations of about 1200 Å of $SiO_2$ ($\lambda/4$ at 4880 Å) are made with the mask in three different positions. In this way the plate is nearly covered with a random patch pattern and the phase variations range from zero to $3\lambda/4$. Some experimentation will undoubtedly be necessary before an appropriate plate is obtained. The plate is then rotated to produce time-varying phase distortions.
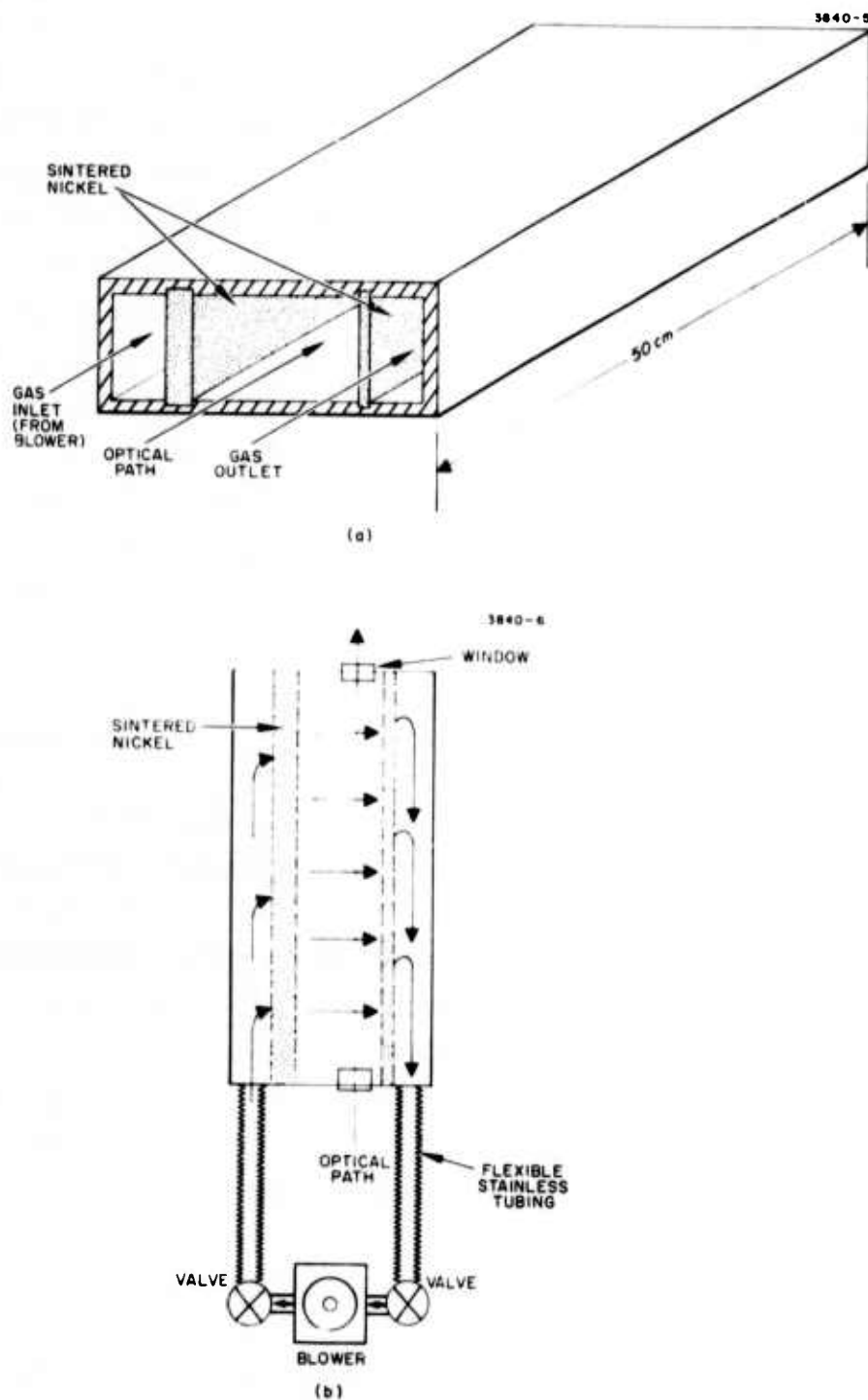
41

Fig. 17. Schematic of flowing gas cell design for
blooming studies. (a) View with endplate
removed showing sintered nickel diffuser
plates. (b) Connection of cell with blower.
Cell is mounted with a vertical optical
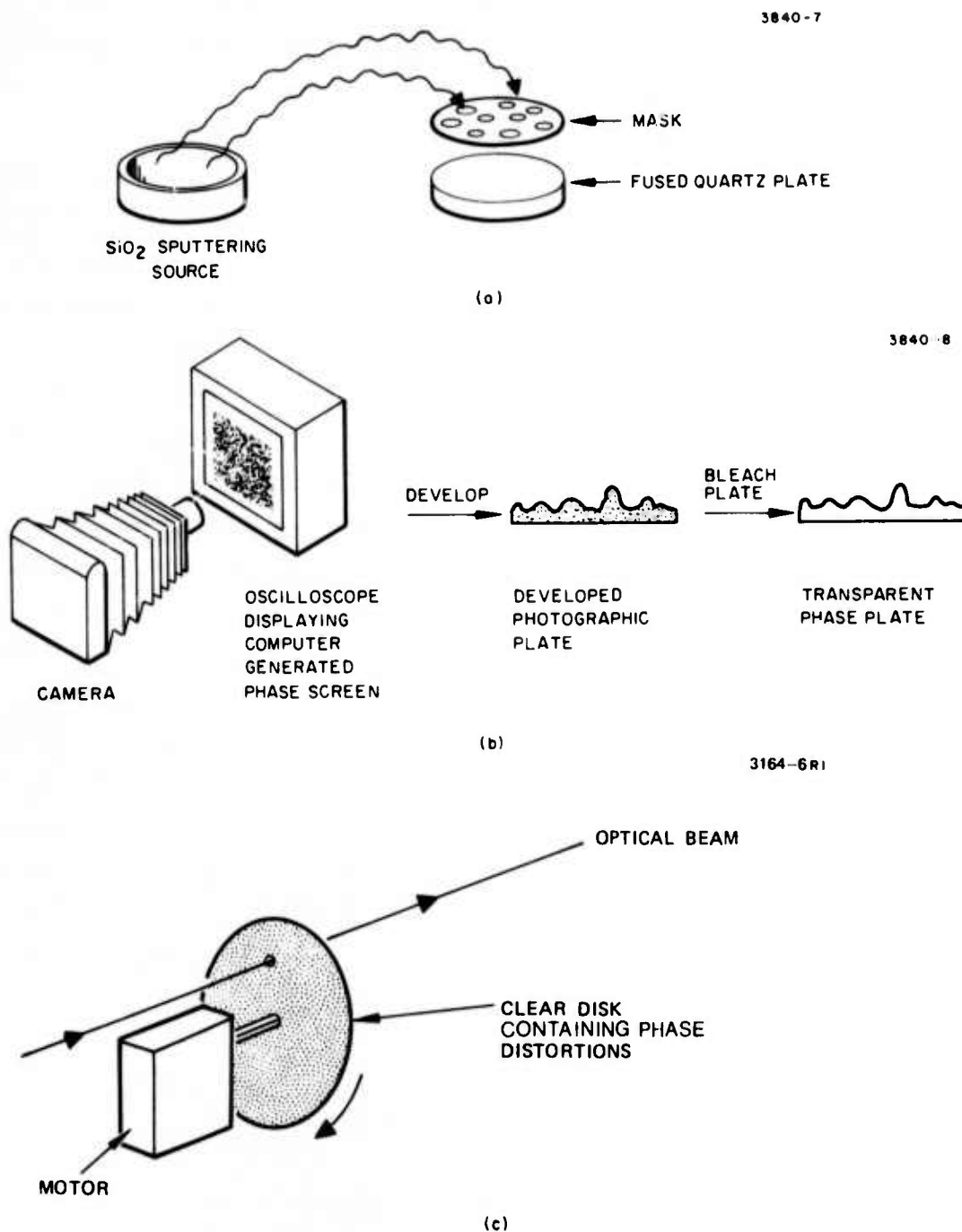path to minimize buoyancy effects.

Fig. 18. Phase screen for generating artificial turbulence effects. (a) Evaporated random patches, $SiO_2$ on a fused quartz substrate. (b) Bleached photographic emulsion exposed using computer-generated phase screen. (c) Motion of screen produced by method (a) or (b) to provide time-varying turbulence.

The advantage of this technique is that it is easily calibrated. The optical thickness variations are known because of the controlled sputtering rate of $SiO_2$. They can also be easily measured with a Sloan Dektak, an electronic height gauge with $\pm 25$ $\overset{o}{A}$ resolution. The disadvantage of this technique is that the phase fluctuations do not have the correct scale sizes to simulate atmospheric turbulence.

The second method for producing the phase screen uses the NOL propagation code to generate an atmospheric phase screen. This screen is displayed on an intensity modulated oscilloscope so that different phase amplitudes produce different intensities on the display. Photographing this display and developing the plate produces a transmission-modulated plate; bleaching the silver from the emulsion leaves a transparent phase-modulation plate whose thickness variations are proportional to the original phase variations produced by the computer and displayed on the oscilloscope.

Obviously, this technique produces a phase screen that when rotated at an appropriate speed can accurately simulate the spatial and temporal characteristics of atmospheric turbulence. The difficulty arises with accurately calibrating the amplitude phase variations. Hopefully, this calibration can be done by either using the Dektak instrument, as with the evaporated plate or in an interferometer. We intend to fabricate and calibrate phase screens using both of these techniques during the next quarter.

# III. PLANS FOR THE NEXT QUARTER

## A. Experimental

During the next quarter we will complete construction of the flowing gas cell, the adaptive pointing and focus controls, and the artificial turbulence generators. A single fixed or moving glint target will be used to study COAT compensation using all of these devices in various combinations. For example, we want to compare blooming compensation using both phase control and pointing and focus control to that observed with only phase control or only pointing/focus control. In addition to testing the flowing gas cell, we plan to repeat the single glint blooming measurements presented in this report, but using a vertical optical path through the gas cell. The goal of these measurements will be a better agreement with computer simulation results.

Complex target studies during the next quarter will concentrate on multiple glint targets in various configurations and with different relative motions. The effect of various receiver geometries on COAT compensation with these targets will be investigated. If time permits we will also study some diffuse targets.

## B. Computer Simulation

The adaptive pointing and focus subroutines will be completed during this next quarter and implemented into the complete COAT simulation code. Comparisons of phase conjugate and multidither COAT algorithms will be made. Studies with moving glint targets will be started and compared to experimental results where practical.

# REFERENCES

1. J. E. Pearson, "Multidither COAT Experimental Results," presented at DARPA/Navy Adaptive Optics Symposium, Lincoln Laboratories, Massachusetts, 3 December 1974.

2. J. E. Pearson, "COAT Measurements and Analysis," contract F30602-75-C-0001, Technical Report No. 1, December 1974. (AD784859).

3. J. E. Pearson, et al, "Coherent Optical Adaptive Techniques," contract F30602-73-C-0248, Technical Report No. 5, December 1974. (AD773189).

4. D. Fouche and A. Pike, private communication.

5. W. P. Brown, Jr. and J. E. Pearson, "Multidither COAT Compensation for Thermal Blooming and Turbulence: Experimental and Computer Simulation Results (U)," presented at 1st DoD Conference on High Energy Laser Technology, San Diego, CA, October 1974.

6. W. P. Brown, Jr., "Report on an Adaptive Optical System Simulation," presented at DARPA/Navy Adaptive Optics Symposium, Lincoln Laboratories, Massachusetts, 3 December 1974.

7. D. Fouche, unpublished.

8. L. C. Bradley and J. Herrmann, Appl. Opt. 13, 331 (1974).

9. R. F. Ogrodnik and G. Gurski, "Target Return — Adaptive Aperture System Interaction Effects (U)," presented at 1st DoD Conference on High Energy Laser Technology, San Diego, CA, October 1974.

10. W. B. Bridges, J. E. Pearson, et al., "Coherent Optical Adaptive Techniques," Contract F30602-73-C-0248, Technical Report No. 3, January 1974. (AD773189).

11. R. J. Roark, Formulas for Stress and Strain, 4th ed. (McGraw-Hill, New York, 1965).

**Preceding page blank**